Journal of Power Sources 359 (2017) 173–181

Contents lists available at ScienceDirect

Journal of Power Sources

journal homepage: www.elsevier.com/locate/jpowsour

Electrochemical performance and interfacial investigation on Si composite anode for lithium ion batteries in full cell

Hitoshi Shobukawa [a, b, *], Judith Alvarado [a, c], Yangyuchen Yang [a, c], Ying Shirley Meng [a]

[a] Department of NanoEngineering, University of California, San Diego, 9500 Gilman Drive, La Jolla, CA 92093, USA
[b] Corporate Research & Development Center, Asahi Kasei, 1-105 Kanda Jinbocho, Chiyoda-ku, Tokyo 101-8101, Japan
[c] Materials Science and Engineering Program, University of California, San Diego, La Jolla, CA 92093, USA

HIGHLIGHTS

- Lithium ion secondary batteries using Si composite anode are investigated.
- High rate capability can be achieved with FEC additive electrolyte.
- A stable SEI composed of inorganic species is formed with FEC additive electrolyte.

ARTICLE INFO

Article history:
Received 29 January 2017
Received in revised form
10 May 2017
Accepted 14 May 2017

Keywords:
Lithium ion battery
Silicon anode
Full cell
SEI

ABSTRACT

Lithium ion batteries (LIBs) containing silicon (Si) as a negative electrode have gained much attention recently because they deliver high energy density. However, the commercialization of LIBs with Si anode is limited due to the unstable electrochemical performance associated with expansion and contraction during electrochemical cycling. This study investigates the electrochemical performance and degradation mechanism of a full cell containing Si composite anode and $LiFePO_4$ (lithium iron phosphate (LFP)) cathode. Enhanced electrochemical cycling performance is observed when the full cell is cycled with fluoroethylene carbonate (FEC) additive compared to the standard electrolyte. To understand the improvement in the electrochemical performance, x-ray photoelectron spectroscopy (XPS), cyclic voltammetry (CV), electrochemical impedance spectroscopy (EIS), and scanning electron microscopy (SEM) are used. Based on the electrochemical behavior, FEC improves the reversibility of lithium ion diffusion into the solid electrolyte interphase (SEI) on the Si composite anode. Moreover, XPS analysis demonstrates that the SEI composition generated from the addition of FEC consists of a large amount of LiF and less carbonate species, which leads to better capacity retention over 40 cycles. The effective SEI successively yields more stable capacity retention and enhances the reversibility of lithium ion diffusion through the interphase of the Si anode, even at higher discharge rate. This study contributes to a basic comprehension of electrochemical performance and SEI formation of LIB full cells with a high loading Si composite anode.

1. Introduction

Rechargeable LIBs are widely used for many types of electronic devices because of their high energy density and longevity [1,2]. Many researchers have focused on high capacity materials to further propel the electrochemical performance, creating the next generation LIBs [3–6]. The current market is dominated by carbon (graphite) anode which offers limited power and energy density (372 mAh g^{-1}). In order to make a significant increase in power density, higher capacity anode materials are required given that carbon materials have already reached their full theoretical capacity.

Silicon (Si) is theoretically expected to have almost 10 times higher capacity than the conventional graphite material (Si: 3579 mAh g^{-1}) [7]. However, Si as an anode poses several challenges such as serious volume change during electrochemical cycling causing rapid capacity decay and continuous electrolyte side reactions on the surface that prevent its stability during cycling

* Corresponding author. Department of NanoEngineering, University of California, San Diego, 9500 Gilman Drive, La Jolla, CA 92093, USA.
E-mail address: shobukawa.net@gmail.com (H. Shobukawa).

http://dx.doi.org/10.1016/j.jpowsour.2017.05.044
0378-7753/

[8–10]. Researchers have investigated several types of Si anodes and binders such as nano sized Si particles, Si imbedded in a carbon matrix, and amorphous Si thin film to overcome these issues [11,12]. While these strategies improve the cycling performance, they have not reached a basic resolution. This is partially due to the solid electrolyte interphase (SEI) which forms on the surface of the anode due to instability of the conventional electrolyte at the lower voltage regime and dictates the electrochemical stability of the anode. The SEI formation is also affected by the large volume expansion and contraction during the charge and discharge, which propagates the sequestration of Li ions at each cycle [13,14]. The morphology and composition of the SEI also depends on the electrolyte components, thus it is crucial to produce a stable SEI on the anode surface to achieve long cycle performance. To enhance the electrochemical stability of Si, vinylene carbonate (VC) [15] and fluoroethylene carbonate (FEC) are extensively used as additives for the standard carbonate electrolyte ($LiPF_6$, ethylene carbonate (EC): diethyl carbonate (DEC)) [16–18]. FEC has favorably been considered a more effective electrolyte additive because it is more effective at stabilizing the capacity retention and lowering the cell impedance. Schroder, Alvarado et al. demonstrated the effect of FEC additive (10 wt%) to the conventional carbonate electrolyte and found that the SEI derived from FEC can effectively improve the discharge capacity retention and coulombic efficiency (C.E.) [19]. According to Mullins and coworkers, the addition of 3 wt% FEC into a EC-based electrolyte demonstrated that capacity retention of the Si anode can slightly improve, albeit, until 20 cycles [16]. However, Lucht and coworkers showed that 5% FEC is not sufficient to form an effective SEI on the Si interface. On the other hand, increasing the FEC percentage to 25% does not further stabilize the electrochemical cycling and increase cell resistance [20]. Given, the extensive studies on the effect of FEC percentage in conventional electrolytes, the addition of gives the best results for increasing capacity retention and C.E [17,19].

Typically, researchers have focused their efforts in investigating the electrochemical performance of Si anode in a half cell, where lithium (Li) metal is used as a counter electrode which contains a limitless supply of Li in the cell. This inherently hides the true electrochemical properties of the anode. Conversely, in a full cell the supply of Li is governed by the cathode material; hence, making it more difficult to maintain the electrochemical performance of the Si composite anode [21–23]. Given what is known about the SEI, during the charge and discharge process the active Li ions are continuously consumed by the SEI on the negative electrode, which can cause devastating effects in a full cell. Dupre and coworkers demonstrated the electrochemical performance and degradation mechanism of the Si composite anode in a full cell using lithium nickel manganese cobalt oxide (NMC) as the cathode [24]. They suggest that the available Li ions are consumed in the SEI or in the electrolyte causing capacity fade for extended cycles. Their study gave a detailed understanding for the decomposition mechanism of Si composite in a full cell when cycled with FEC. However, previous full cell studies fail to reveal the actual effect of FEC additive to the electrolyte because their work do not compare the results with an electrolyte not containing the additive [24–26]. A systematic comparison of the standard electrolyte and FEC additive electrolyte has yet to be studied. One must fully understand if the effect of FEC is also positive when used in a full cell with Si anode and the cathode to further verify the use of FEC additive in commercial cells.

In this study, we compare the electrochemical performance of the Si composite anode full cell in $LiPF_6$/ethylene carbonate (EC)/diethyl carbonate (DEC) and $LiPF_6$/EC/DEC/FEC (10 wt%). The detail influence of FEC additive on the electrochemical reaction of the full cell is investigated by means of cyclic voltammetry (CV). Electrochemical impedance spectroscopy (EIS) measurement is used to determine effect of FEC in the electrolyte on the overall impedance of the cell after electrochemical cycling and XPS is used to characterize the chemical components of the SEI on the Si composite anode. Given the transition metal instabilities of NMC during electrochemical cycling, researchers have focused their efforts on $LiFePO_4$ (LFP) to enhance the electrochemical performance in both half cells and full cells [27–30]. Until now, LFP has been one of the most versatile, stable, and promising cathode materials. Therefore, to isolate the effects of Si anode and its SEI in a full cell, LFP is utilized in this study. LFP has been extensively studied in a half cell in the literature, the results suggest that the LFP cathode is stable upon prolonged cycling. This is reflected by the negligible iron dissolution and reduced formation of the cathode electrolyte interphase, therefore, the resistance within the cell during electrochemical cycling of the half cell is negligible. Moreover, this has been verified by XPS and electrochemical analyses [27,31,32]. Herein, we discuss the difference between the full cell cycled in $LiPF_6$/EC/DEC and $LiPF_6$/EC/DEC/FEC. CV measurement gives insight to highly reversible lithium ion diffusion into the Si SEI for electrodes cycled with FEC at high scan rate. Si electrodes cycled with FEC have higher amounts of LiF and less carbonate species compared to electrodes cycled without FEC, contributing to the improvement of the full cell battery performance.

2. Experimental methods

2.1. Electrode fabrication

Si nanoparticle (Alfa Aesar, average particle size: 50 nm) was used as the active material of negative electrode. The Si composite anode was fabricated as follows: 50 wt% nano-Si powder, 25 wt% Ketjenblack (Akzo Nobe: EC-600JD), and 25 wt% sodium carboxymethyl cellulose (CMC-Na, DS = 0.9, Mw = 250,000, Sigma Aldrich) were mixed in water. The obtained slurry was coated on Cu foil by using a doctor blade and dried at 100 °C for 20 h under a vacuum to completely dry any water on the surface. The electrode sheet was cut into a disk and applied for the battery test. The mass of the Si active material on the electrode was 0.5 mg of Si per cm^2. The positive electrode was prepared as follows: 80 wt% $LiFePO_4$ powder (MTI Corporation), 10 wt% carbon black (Timcal, Super-P) and polyvinylidene fluoride (PVDF) were mixed in *N*-methyl-2-pyrrolidone (NMP) as solvent to prepare a slurry. The obtained slurry was coated on Al foil by using a doctor blade and dried at 100 °C for 20 h under a vacuum to completely dry any NMP on the surface. These electrodes were used to assemble the 2032 coin cell using a polymer separator (C480, Celgard Inc., USA). The electrolyte (Battery grade, BASF) was a solution of 1 M $LiPF_6$ dissolved in EC/DEC 1:1 (wt%): Selectilyte LP 40 and EC/DEC/FEC 45:45:10 (wt%): Selectilyte A6 where $LiPF_6$/EC/DEC and FEC stand for ethylene carbonate, diethyl carbonate, and fluoroethylene carbonate, respectively. Coin cells were assembled in a glovebox purged with high purity Ar gas and maintained with water vapor levels at or less than 5 ppm.

2.2. Electrochemical test

After the coin cells were assembled, electrochemical performance tests were performed using an Arbin battery cycler in galvanostatic mode. The charge and discharge performance of the full cell was conducted between 2.5 V and 3.5 V. The open circuit voltage of the coin cells was monitored for 10 h and then we started to charge and discharge the cell with the current density of 60 μA cm^{-2}, which is approximately corresponding to a C-rate of C/15. The percent capacity retention was calculated with respect to the first discharge capacity. Cyclic voltammetry (CV) measurements

were carried out at a sweep rate of 0.1 mV $s^{-1}$and 1 mV s^{-1}. Additional electrochemical impedance spectroscopy (EIS) measurements were conducted over the frequency range scanned from 1 MHz to 0.01 Hz at the fully lithiated states. The impedance was collected by using Biologic SP-200 electrochemical interface after the first cycle, 20th cycle and the 40th cycle. ZView software was used to fit the collected EIS spectra to the equivalent circuit. A three-electrode Swagelok cell configuration was used for the EIS measurement. Si active material was the working electrode, and Li metal served as the counter and reference electrode. The three electrode cell allows for proper isolation of the working electrode impedance. It was first lithiated at a cell potential of 0.05 V and then it was carried out with EIS measurement, as described earlier. All electrochemical measurements were carried out at 20 °C.

2.3. Scanning electron microscopy (SEM)

After the electrochemical cycling test, coin cells were disassembled and the Si anodes were rinsed with DEC to remove the electrolyte residual and dried in the Ar-filled glovebox. The surface images of the Si anode were collected with a field emission environmental scanning electron microscope (Philips XL30).

2.4. X-ray photoelectron spectroscopy (XPS)

XPS was performed at the Laboratory for Electron and X-ray Instrumentation at UC Irvine, using a Kratos AXIS Supra. In order to avoid air exposer, the samples were prepared in the glovebox connected to the XPS. Samples were transferred from the glove box to the XPS from argon atmosphere to ultra-high vacuum greater than 10^8 torr. XPS was operated using Al anode source at 15 kV.

All XPS measurements were collected with a 300 μm by 700 μm spot size without using a charge neutralizer during acquisition. Survey scans were collected with a 1.0 eV step size followed by high-resolution scans with a step size of 0.05 eV, for carbon 1s, oxygen 1s, lithium 1s, fluorine 1s, silicon 2p, and phosphorus 2p regions.

Fits of the XPS spectra were performed with CasaXPS software (version 2.3.15, Casa Software Ltd.) to estimate the atomic compositions and chemical species comprising the SEI. All fitting followed a self-consistent method similar our previous publication. (cite all of our previous work and recent published papers) All SEI species were assumed to be electronically insulating, therefore, fitted with linear backgrounds and with Voight functions composed of 15% Lorentzian and 85% Guassian. Initial peak fits were made of the spectra using a Levenberg–Marquardt least-squares algorithm, and atoms in the same functionality were assumed to be stoichiometric [19,33,34]. The resulting spectra were then refit and all spectra were shifted relative to the binding energy of the carbon 1s sp [3] (assigned to 284.8 eV) to compensate for any off-set during the measurement.

3. Results

3.1. Electrochemical characterization

It is difficult to make an in house full cell, balancing the weight of both the anode and cathode. In some practices, the matched capacity electrodes are purchased and assembled in a laboratory setting. In our case we make both the anode and cathode, match the capacity and assemble the full cell. Given the difficulty, we wanted to ensure that we were able to assemble a proper working full cell with LFP vs MCMB graphite. The cycling performance is consistent with the proper working capacity and demonstrates suitable coulombic efficiency (Fig. 1S (a)). Prior to investigating the electrochemical performance of the lithium ion full cell, we show the initial cycle performance of lithium half cells for both Si anode and LFP cathode materials cycled with $LiPF_6$/EC/DEC (Fig. 1 (a)). The lithiation capacity of Si anode in a half cell is 1.48 mAh and the delithiation capacity of LFP is 1.30 mAh, demonstrating that the capacity of the Si anode is 1.13 times higher than that of LFP cathode. Furthermore, it shows that both cathode and anode electrodes perform adequately.

Si anode is combined with the LFP cathode to fabricate a lithium ion full cell and is tested using $LiPF_6$/EC/DEC and $LiPF_6$/EC/DEC/FEC to compare the electrochemical performance of each cell. Fig. 1 (b) shows the typical initial charge and discharge voltage profiles of the lithium ion full cell within the potential window of 2.5 V–3.5 V at C/15 rate. Both electrolytes show an inflection in the voltage profile around 2.7 V and show a distinctive plateau at 3.3 V. The coulombic efficiency (C.E.) for the first cycle is 61.2% and 60.0% for $LiPF_6$/EC/DEC and $LiPF_6$/EC/DEC/FEC electrolyte, respectively. Among these electrolytes, the C.E. of the cell cycled with $LiPF_6$/EC/DEC/FEC is slightly lower than that of the cell cycled with $LiPF_6$/EC/DEC, consistent with half cell work found in the literature [33,34]. The irreversible capacity is known to originate from the rapid decomposition of the FEC additive to form the SEI on the surface of Si anode. A small shift observed around 1.8 V of the cell cycled in $LiPF_6$/EC/DEC/FEC is assumed to be associated with the irreversible reaction of FEC to form a more inorganic SEI.

To understand the electrochemical reactions that occur during cycling in better detail, cyclic voltammetry (CV) studies were conducted to compare the effects each electrolyte. Fig. 2 (a) shows the various full cell CV profiles for the cell cycled in $LiPF_6$/EC/DEC measured over the potential window of 2.5 V and 3.5 V using 0.1 mV s^{-1} scan rate. In general, the first scan process involves the SEI formation from the decomposition of EC and DEC at a voltage range of 2.7–2.9 V (Fig. 2 (a)). The sharp peak at 3.4 V corresponds to the intercalation and deintercalation process of the Li ion into the electrodes. During the subsequent cycles, specifically the large sharp peak at 3.4 V found in the first cycle decreased and a new peak emerged at 3.25 V. This peak remains stable throughout cycling, similar to the behavior of the Si anode electrochemical reaction in half cell, shown in Fig. 1S (b).

Conversely, Fig. 2 (b) shows that the full cell cycled in $LiPF_6$/EC/DEC/FEC demonstrated an additional peak in the CV around 1.8 V, corresponding to the decomposition of FEC seen in the inset. As shown in Fig. 1S (c), the FEC decomposition can be clearly seen in the CV of Si half cell, but is not seen in the CV of LFP half cell [34,35]. This validates that the FEC decomposition only occurs on the Si anode surface. Therefore, the two peaks presented at around 1.9 V and 2.3 V in the CV can be attributed to the FEC reduction because it is known to decompose prior to EC or DEC to form an effective SEI. For the full cell cycled in the $LiPF_6$/EC/DEC electrolyte, oxidation and reduction peaks in the second cycle are shown at around 3.252 V and 2.901 V, the potential separation between peaks is 0.351 V (Fig. 2 (a)). Subsequent cycling reveals that the peak separation increases to 0.512 V in the 25th cycle. On the other hand when the cell is cycled in the $LiPF_6$/EC/DEC/FEC electrolyte as shown in Fig. 2 (b), the potential separation between the oxidation and reduction peaks in the second cycle and 25th cycle are 0.333 and 0.338 V. The difference of the potential separation for the $LiPF_6$/EC/DEC/FEC is smaller than that of $LiPF_6$/EC/DEC, indicating that lithium ions and electrons are more electrochemically active due to the conditions of the electrode-electrolyte interface.

To understand the difference in the interface generated from each electrolyte the full cells were cycled at higher scan rate (1 mV s^{-1} scan rate), shown in Fig. 3. It is clearly shown that the addition of FEC to the electrolyte improves the reversibility of lithium ion than that of standard electrolyte (Fig. 3 (a) and (b)). It is

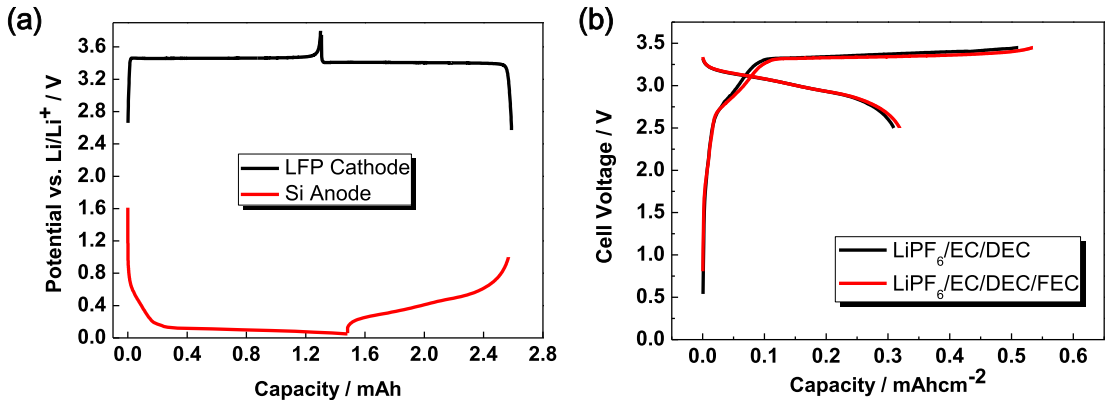

Fig. 1. (a) First cycle voltage profiles of lithium half cells for both LFP cathode (Coulombic efficiency: 99.0%) and Si anode cycled with $LiPF_6$/EC/DEC (Coulombic efficiency: 73.4%). (b) Charge and discharge voltage profiles of lithium ion full cell at the first cycle between 2.5 V and 3.5 V cycled with $LiPF_6$/EC/DEC and $LiPF_6$/EC/DEC/FEC.

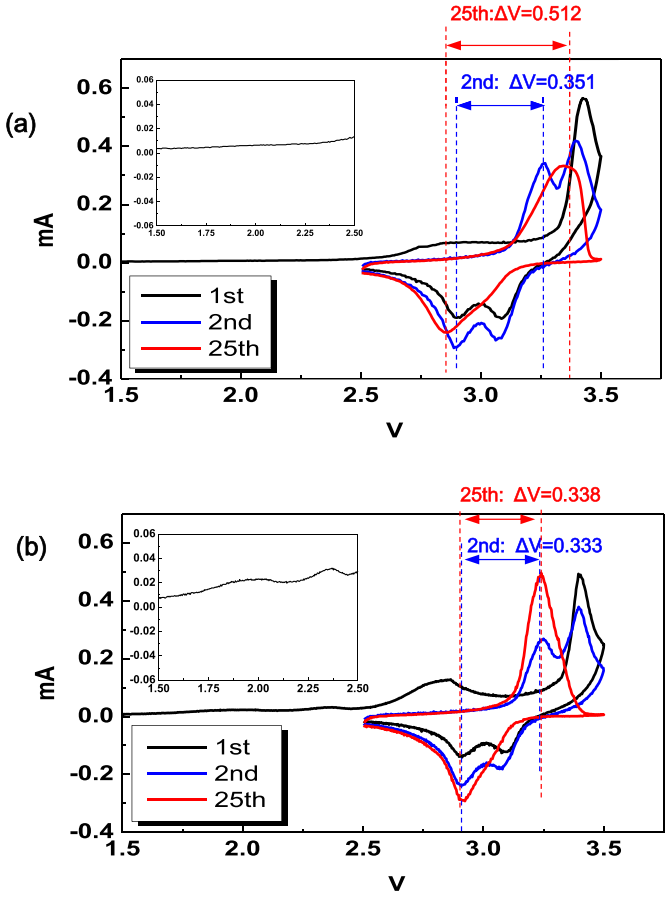

Fig. 2. CV of Si anode full cell with (a) $LiPF_6$/EC/DEC and (b) $LiPF_6$/EC/DEC/FEC at 0.1 mV s^{-1}.

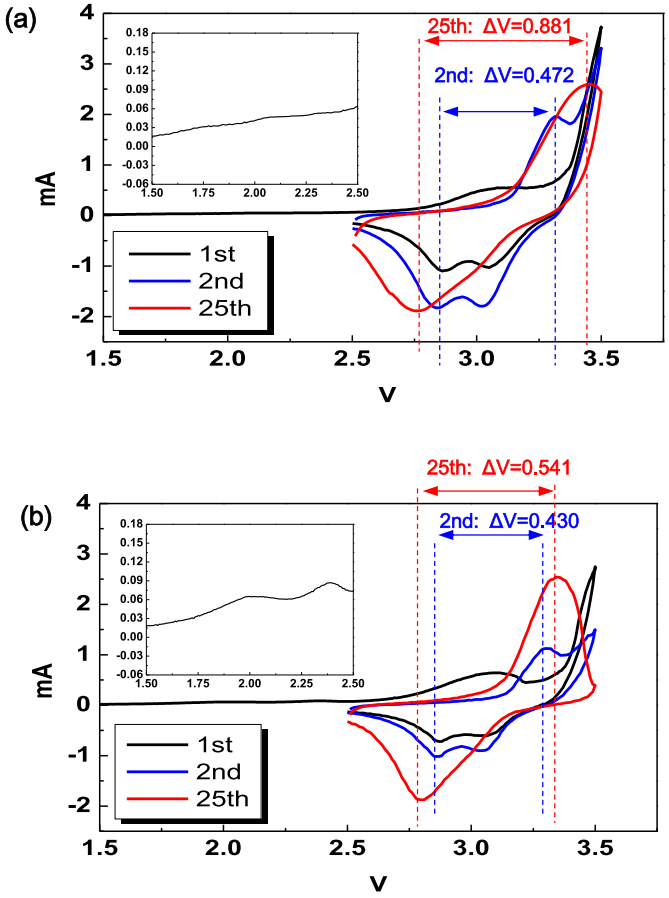

Fig. 3. CV of Si anode full cell with (a) $LiPF_6$/EC/DEC/FEC and (b) $LiPF_6$/EC/DEC at 1 mV s^{-1}.

also obvious that the difference of the potential separation for the $LiPF_6$/EC/DEC electrolyte is 0.209 V, which is much larger than that of the $LiPF_6$/EC/DEC/FEC electrolyte (0.111 V). These results suggested that the reversibility and reactivity of the full cell with $LiPF_6$/EC/DEC/FEC are improved due to the enhancement of the lithium ion diffusion and electronic conductivity due to the reductive products generated by FEC on the anode surface.

Fig. 4 compares the discharge capacity retention and C.E. of the full cells cycled with $LiPF_6$/EC/DEC and $LiPF_6$/EC/DEC/FEC electrolyte at a C/10 rate. Although the full cell cycled with $LiPF_6$/EC/DEC exhibits higher discharge capacity in the earlier cycles (0.51 mAh cm^{-2}), the capacity gradually begins to decrease after the tenth cycle. By the 40th cycle the capacity retention dramatically decreases to 39% with capacity of 0.21 mAh cm^{-2}, ultimately, leading to poor electrochemical performance. On the other hand, the cells cycled with $LiPF_6$/EC/DEC/FEC shows quite stable capacity retention, achieving a discharge capacity of 0.34 mAh cm^{-2} after 40 cycles with 75% capacity retention. This confirms that the addition of FEC to the electrolyte can be useful to enhance the electrochemical performance of the Si anode full cell as well as in the

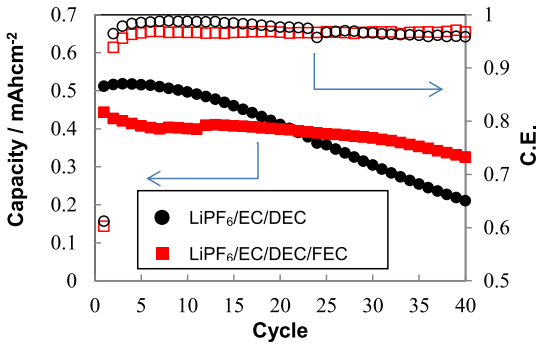

Fig. 4. Cycling performance of capacity retention and coulombic efficiency for 40 cycles of the full cell cycled with $LiPF_6$/EC/DEC, $LiPF_6$/EC/DEC/FEC.

graphite anode full cell [36].

3.2. Electrochemical impedance spectroscopy (EIS)

To further prove the effect of the FEC additive and factors that contribute to the full cell electrochemical enhancement, EIS measurements were performed. First we focus on the effect of FEC additive on the Si electrode interface by using three-electrode Swagelok cell. Fig. 3S (a) and (b) show the Nyquist plot of the counter electrode (Li) and working electrode (Si) when cycled with $LiPF_6$/EC/DEC and $LiPF_6$/EC/DEC/FEC electrolytes after first lithiation. Each of these plots are composed of a semicircle in high frequency region, second semicircle in middle frequency region and a slope in the low frequency region, which are attributed to the SEI resistance, charge transfer resistance and Warburg impedance, respectively. There were remarkable differences in the size of semicircle between $LiPF_6$/EC/DEC and $LiPF_6$/EC/DEC/FEC electrolytes.

The impedance of the Si electrode for $LiPF_6$/EC/DEC is increased in comparison with that of $LiPF_6$/EC/DEC/FEC because the Si electrode cycled with $LiPF_6$/EC/DEC is assumed to be thicker than that of $LiPF_6$/EC/DEC/FEC [16]. This same phenomenon can be seen in the counter electrode lithium metal. As a result, FEC decomposes to form an effective SEI with lower cell interfacial resistance. Moreover, note that the impedance of Li metal has a significant contribution to cell resistance, as a result it is important to take that into consideration when measuring the cell resistance in half cells. Now that we know how FEC affects the resistance on the Si anode, we further evaluate the fundamental resistance in the full cell. Fig. 5 (a and b) shows the impedance spectra (Nyquist plot) of the cells cycled with $LiPF_6$/EC/DEC and $LiPF_6$/EC/DEC/FEC electrolytes after the 1st, 20th and 40th cycle in the charged state. The equivalent circuit parameter shown in Fig. 5 (c) fitted for Rs, the resistance of the bulk electrolyte, R_{SEI} which is the resistance of the SEI and Rct which is the charge transfer resistance of the intercalation process between the electrodes and the electrolytes. The Warburg impedance is due to the solid state lithium ion diffusion into the electrode. The clear difference in the impedance spectra between the full cell cycled in the $LiPF_6$/EC/DEC and $LiPF_6$/EC/DEC/FEC is the SEI resistance, summarized in Fig. 5 (c). Since these EIS experiments were conducted in a two electrode cell, the spectra include the impedance of both Si anode and LFP cathode. This makes it difficult to isolate the effects of each electrode, however, we wanted to ensure that we tested the full cell as it would be commercially made. The R_{SEI} gives a clear indication of the health and stability of the full cell which is why we focus more on this aspect. It is also considered that the resistance of LFP is more stable, allowing us to think more about the influence of the Si anode in the system. The R_{SEI} in the first cycle for the cell cycled with $LiPF_6$/EC/DEC is 12.69 Ω which is slightly larger than that of the cell cycled with $LiPF_6$/EC/DEC/FEC (11.2 Ω). After subsequent cycles the R_{SEI} of $LiPF_6$/EC/DEC becomes significantly larger compared to the cell cycled with $LiPF_6$/EC/DEC/FEC. Further examination of the Rct, we find a significant difference between the cells cycled with $LiPF_6$/EC/DEC and $LiPF_6$/EC/DEC/FEC. Rct is usually affected by the kinetics of lithium ion diffusing on the interface between the SEI and Si anode surface, which might be related to the electrode morphology or SEI components [37]. As a result, in the presence of FEC the impedance decreased over prolonged cycles compared to its electrolyte counterpart, demonstrating that FEC helps form an effective SEI, positively affecting the electrochemical performance.

3.3. Surface morphology of Si composite anode after cycling (SEM)

The morphology of the Si composite anode after prolonged cycles was investigated by SEM. Fig. 6 (a) shows an image of the pristine (uncycled and unassembled electrode) Si composite anode, which is composed of Si nano powder mixed well with Ketjen black and CMC binder at a weight ratio of 2:1:1. The Si anode cycled in $LiPF_6$/EC/DEC after 40 cycles clearly demonstrates significant particle agglomeration (Fig. 6 (b)). Furthermore, there is also severe cracking in the Si composite anode after the insertion of lithium ions; ultimately, increasing the polarization of electrode and poor electric network between active material particles and conductive additives or copper foil current collector. These effects are inherently seen in the supporting information (Fig. 2S), demonstrating the large overpotential and capacity fade occur when the cell is cycled without FEC, making it difficult to maintain good capacity retention and stable C.E. On the other hand, when the full cell was cycled with $LiPF_6$/EC/DEC/FEC to 40 cycles, large amount of Si particle aggregates without large crack formations are found on the electrode surface (Fig. 6 (c)). The comparison of the SEM images between the two electrodes after cycling further confirms that SEI generated with the addition of FEC effectively stabilizes the full cell performance significantly because the FEC decomposition products are believed to suppress the generation of the newly exposed surface by maintaining the structural integrity in the Si composite anode in the initial cycles [33,34].

There are several factors the affect the performance of the Si anode, one of which is due to the different surface morphology shown in Fig. 6; however, when the full cell was investigated at a high CV scan (1 mV s^{-1}) there is a significant difference at the 10th cycle between the electrolytes. The reason for capacity fade may not be only the surface degradation but also the degree of the lithium migration into the surface of the Si composite anode. The poor lithium migration should be related to the surface condition. Surface chemistry might affect the electrochemical performance, which vary the kinetics of lithium ion migration through the interface of the electrode.

As a result, these investigations indicate that the SEI comprised from the addition of FEC would prevent the electrolyte from further decomposition and maintain the lithium ion diffusion into the SEI to some extent. To further investigate the relationship between surface chemistry and electrochemical behavior of the full cell cycled with $LiPF_6$/EC/DEC and $LiPF_6$/EC/DEC/FEC, XPS measurements were performed on the Si composite anode after 1st and 40th lithiation.

3.4. Surface analysis of the cycled Si composite anode by XPS

It is important to understand the surface chemistry that occurs as a result of electrolyte degradation because the SEI components play a significant role in electrochemical performance. The cycled

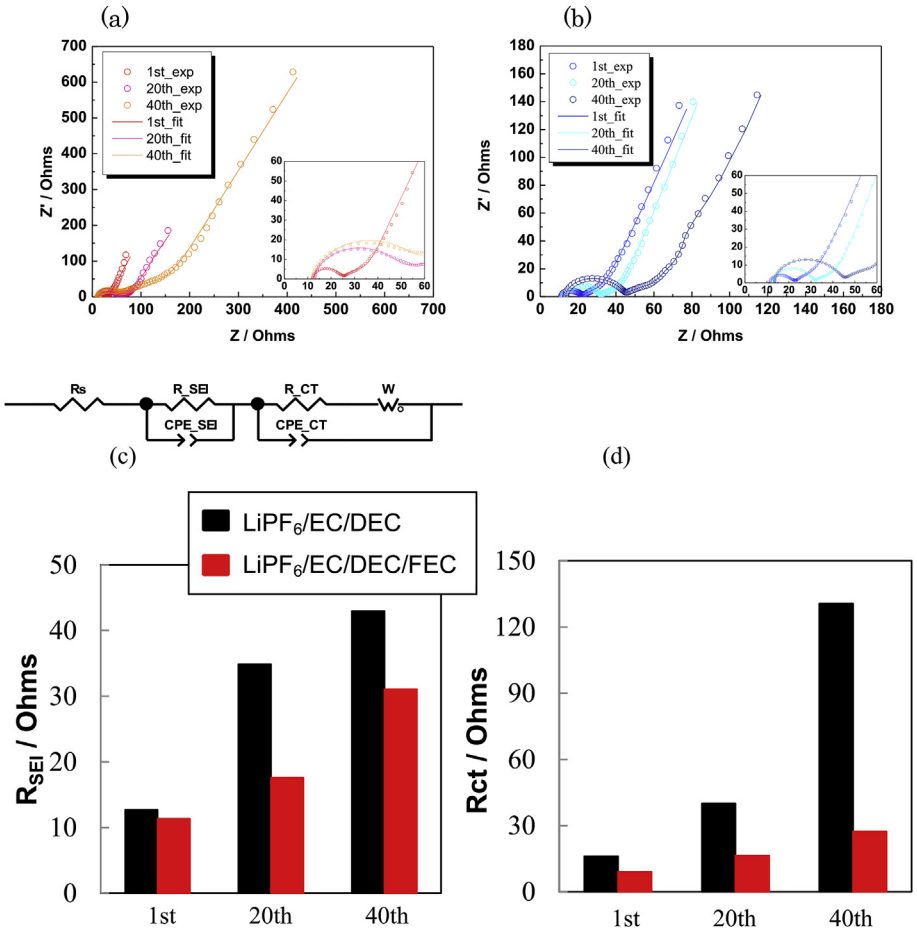

Fig. 5. EIS spectra of fully charged full cell cycled in (a) $LiPF_6$/EC/DEC and (b) $LiPF_6$/EC/DEC/FEC after 1st, 20th and 40th cycle. The fits for the data of each full cell are shown as (c) R_{SEI} (Ω) and (d) Rct (Ω) of the full cells at 1st, 20th and 40th cycled with $LiPF_6$/EC/DEC (black) and $LiPF_6$/EC/DEC/FEC (red). (For interpretation of the references to colour in this figure legend, the reader is referred to the web version of this article.)

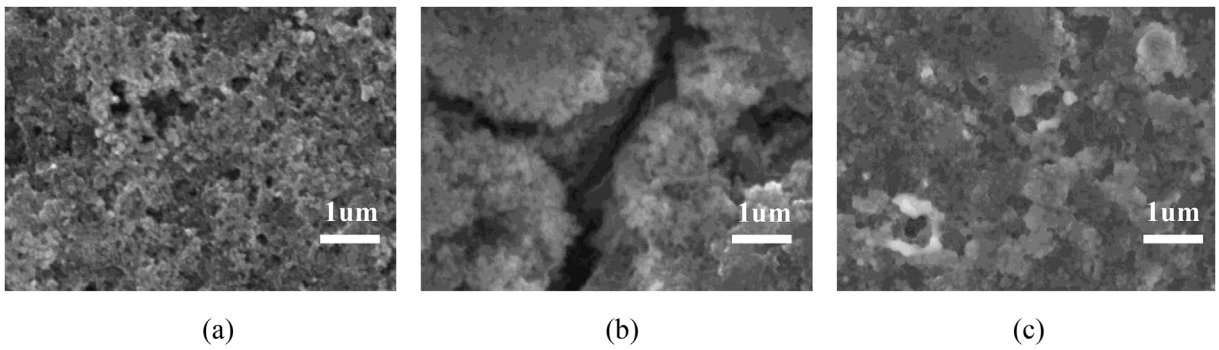

Fig. 6. SEM images of Si anode surface at (a) Pristine state, cycled with (b) $LiPF_6$/EC/DEC and (c) $LiPF_6$/EC/DEC/FEC after 40 cycles.

electrodes were characterized by XPS at the lithiated state for the 1st and 40th cycle when cycled in $LiPF_6$/EC/DEC and $LiPF_6$/EC/DEC/FEC. The electrodes were washed with DEC to make sure that there is no remaining Li salt or solvent residue on the electrodes. Detailed scans of all prepared Si anodes are collected from the C 1s, O 1s, F 1s and Li 1s and P 2p spectra (shown in supporting information). Herein, we focused on the surface species of the Si composite anode because of the stability of LFP. The stability of the cathode is demonstrated in the survey scans of the cycled Si anode in both electrolytes. The low resolution survey demonstrates that there is no "cross talk" between that cathode and the anode, with no clear Fe peaks after 40 cycles. These results lead us to believe that the degradation mechanism solely comes from the Si anode.

As shown in Fig. 7, the high resolution of O 1s spectra demonstrate the electrolyte decomposition components generated from cycling the cells with $LiPF_6$/EC/DEC and $LiPF_6$/EC/DEC/FEC electrolyte. The oxygenated compounds include carbonate, carbonyl, ether, LiO_x and OPF species. This result is quite consistent with the experiment performed by Edstrom et al. and Schroder et al. [19,38] The O 1s spectra of each electrolyte correspond to the species found

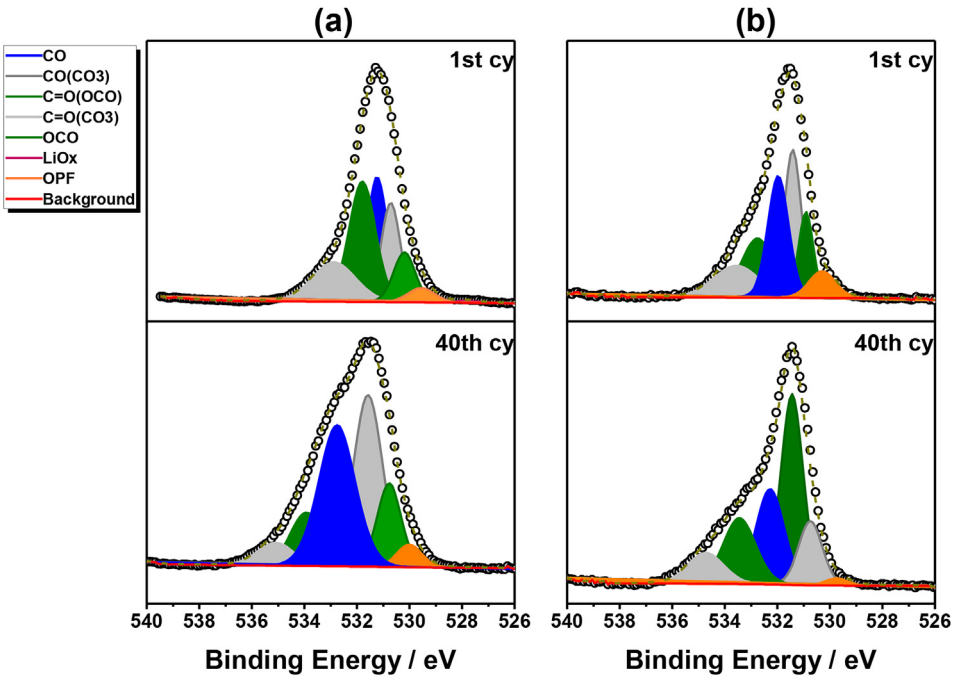

Fig. 7. High resolution O 1s spectra of the Si composite electrolyte decomposition products the after 1st cycle and 40th cycle with (a) $LiPF_6$/EC/DEC and (b) $LiPF_6$/EC/DEC/FEC.

in the C 1s as shown in Fig. 4S. When the cell is cycled with $LiPF_6$/EC/DEC/FEC there is a reduction in CO species, which is mainly generated by the EC decomposition. The P 2p spectra are similar and contain two peaks, one around 134 eV related to OPF and the other 136 eV related to $Li_xP_yF_z$ in Fig. 5S. However the intensity of LixPyFz for the Si anode cycled with $LiPF_6$/EC/DEC electrolyte is larger than that of $LiPF_6$/EC/DEC/FEC electrolyte. This result would suggest that cycling the cell without the addition of FEC results in more $LiPF_6$ decomposition.

4. Discussion

The effect of the FEC additive on full cell electrochemical performance when using Si composite anode and LFP cathode is discussed here. Conducting CV experiments on full cells evaluates the electrochemical behavior and electrode kinetics of the active materials. An important feature is the difference between the first cycle and subsequent cycles shown in Fig. 2 (a), where the peak at 3.25 V in the first cycle shifts to a slightly higher potential in subsequent cycles because of the cell overpotential. Potential difference allows one to determine reversibility of lithium ion intercalation and deintercalation process. For the cell cycled without FEC, the potential separation between the anodic and cathodic peak of 2nd cycle and 25th cycle is nearly 0.161 V. Conversely, Fig. 2 (b) shows no significant difference in the potential difference for the cell cycled in $LiPF_6$/EC/DEC/FEC. In addition, the current intensity of the $LiPF_6$/EC/DEC/FEC can be maintained even at the 25th cycle while there is a drastic drop in current intensity when the cell is cycled with $LiPF_6$/EC/DEC. The effect of FEC is clearly confirmed even at a faster scan rate (Fig. 3). In the case of $LiPF_6$/EC/DEC, the potential difference is 0.209 V at a scan of 1 mV s^{-1}, which is almost twice that of $LiPF_6$/EC/DEC/FEC (0.111 V). Fig. 3 (a) also shows that the peak intensity decreases and the shape of the peak is clearly distorted after 25 cycles, while the peak integrity is maintained when the cell is cycled with $LiPF_6$/EC/DEC/FEC. This suggests that $LiPF_6$/EC/DEC/FEC electrolyte effectively restrains the overpotential during cycling by maintaining the higher reversibility of lithium ion diffusion between the Si anode and the SEI. The reversibility of the electrode should be affected by the interfacial impedance and electrode morphology. The EIS results demonstrate that the impedance of the cell cycled with $LiPF_6$/EC/DEC increased after cycling, which leads to significant capacity decay because the unstable SEI formation increasing the surface film resistance. This result is in good agreement with the study calculated by Soto et al., which suggest FEC produces less short oligomer products compared to EC which produces a thick organic layer that increases the surface resistance [39]. As discussed above, the electrode surface of the Si anode cycled in $LiPF_6$/EC/DEC (Fig. 6 (b)) has severe cracks which cause significant capacity decay during electrochemical cycling. According to Edstrom and coworkers, the Si nanoparticle electrodes cycled with $LiPF_6$/EC/DEC has an uneven SEI. Therefore, it is highly likely that in our study we have low kinetic Li ion diffusion through the Si anode SEI during electrochemical cycling, consistent with high charge transfer resistance. On the other hand, the homogeneous SEI decomposed from $LiPF_6$/EC/DEC/FEC can prevent the Si anode from cracking, as a result, lithium ion diffusion into the electrode improves the coulombic efficiency. This in-depth electrochemical measurement demonstrates that the decomposition products derived from FEC might be effective not only for enhancement the lithium ion diffusion through SEI but also alleviating the undesired extra side reactions on the surface of the Si anode. Here we believe that the FEC decomposition components play an important role to keep the electrochemical performance stable for the full cell as shown in the half cell.

It is expected that the surface chemistry is closely related to the electrochemical behavior. In this regard, the addition of FEC might contribute to protect the Si nanoparticles from having direct contact with the electrolyte by generating a LiF rich SEI layer at the beginning of the electrochemical cycling. This is demonstrated by Sina, Alvarado et al., where STEM/EELS clearly shows that in the first lithiation process the addition of FEC forms a uniformly dense

SEI that maintains the Si particle integrity [33]. Conversely, the Si anode cycled without FEC had a porous nonuniform SEI that exposed the Si particles to the electrolyte, demonstrating the lack of electrode stability. The difference between $LiPF_6$/EC/DEC and $LiPF_6$/EC/DEC/FEC on the surface reaction might affect the electrochemical performance, therefore, XPS surface analysis were conducted.

After 40 cycles, several chemical reactions are involved in the SEI growth process and these reactions generate organic and inorganic type components on the Si anode. The above demonstrated XPS results of the Si composite anode enabled us to understand the important mechanism of the surface chemistry. The relative elemental compositions of the surface after 40 cycles obtained from the XPS measurement are summarized in Fig. 8. From these results, significant difference in the elemental composition can be observed between $LiPF_6$/EC/DEC and $LiPF_6$/EC/DEC/FEC. It should be noted that the atomic percentage of C species at the surface of the electrode may also have contributions from the conductive additive. However, given that XPS probes the first 10 nm of the surface, it is likely that most of the signal comes from the electrolyte decomposition products. The SEI generated from the decomposition of $LiPF_6$/EC/DEC has more carbon species when comparing it to the $LiPF_6$/EC/DEC/FEC electrolyte decomposition. This might be because of the EC decomposition products primarily forming carbon containing species such as carbonate, carbonyl, and ethers. The ratio of OPF species between the first cycle and 40th cycle for the cell cycled with $LiPF_6$/EC/DEC is also larger than that of the cell cycled with $LiPF_6$/EC/DEC/FEC (Fig. 8S). The OPF is assumed to be an indication of $LiPF_6$ decomposition, which might become the resistive species on the surface of the Si composite anode. The accumulations of these types of decomposition compounds on the Si anode surface significantly increases the impedance and degrade the cycle performance [19,38]. On the other hand, FEC is more reactive and decomposes at earlier reduction potential compared to EC or DEC at 1.8 V to form a more resistive SEI. Fig. 8 shows that the amount of F and Li for the cycled with $LiPF_6$/EC/DEC/FEC are higher than that of $LiPF_6$/EC/DEC, corresponding to LiF formation. Some studies have shown that the higher amount of inorganic components, like LiF is correlated to the improvement in electrochemical performance and reversibility of lithium ion diffusion [34,35,40]. Previous DFT calculations enabled one to further understand the FEC decomposition mechanism. According to Balbuena and coworkers, a ring-opening mechanism of FEC at the carbon-ether oxygen bond lead to form LiF as a main reduction product [41,42]. Investigating different current density may lead us to understand how rate affects the surface chemistry on Si anode. In our study we measured CVs at a higher scan rate, where the FEC additive improved the reversibility of lithium ion compared to the electrolyte without FEC. In our galvanostatic cycling we used only one current density to understand the surface chemistry with XPS, so it would be interesting to investigate the effect on current density on SEI composition. Anyway, we believe that these abovementioned effects of FEC additive can successively hamper the increase of the cell impedance and improve the capacity retention and C.E. in full cells.

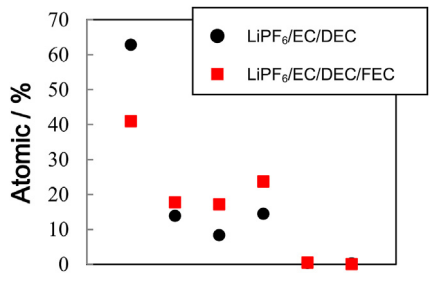

Fig. 8. Elemental composition of the SEI on the Si composite anode after 40 cycles in $LiPF_6$/EC/DEC and $LiPF_6$/EC/DEC/FEC.

In our study, the comparison of the SEI between $LiPF_6$/EC/DEC and $LiPF_6$/EC/DEC/FEC is demonstrated and the FEC additive electrolyte is more effective in improving the electrochemical performance. However, we do begin to see that the capacity retention of the $LiPF_6$/EC/DEC/FEC electrolyte gradually begins to decay because it seems that some of available lithium ion is consumed or trapped in the SEI, consistent with work demonstrated by Dupre and coworkers [24]. Unstable organic species due to the degradation of the EC and DEC solvent might be lithiated on the surface of the Si composite anode during cycling leading to poor retention. In a half cell the supply of lithium ion is limitless, even if lithium ions are consumed by the decomposed organic species, the Li ions flows consistently from the counter electrode (Li metal) allowing the Si anode to cycle over 100 cycles building a continuous SEI eventually increasing impedance in the cell.

To overcome this issue, further improvement is necessary to form a stable SEI on the Si anode surface. The addition of FEC to the conventional electrolyte is not enough to further improve the Si anode full cell. Even if FEC additive is used in the electrolyte for full cells, organic species decomposed will eventually sequester lithium ions after prolonged cycles, demonstrated in this work and by others [24]. Therefore, it is important to seek other more effective electrolytes that would avoid the continuous decomposition of organic species and prevent the extra lithiation on the interface. Moreover, electrode surface modification techniques might also be effective in order for the Si composite anode to prevent the excess degradation of organic electrolyte. Or one could improve the full cell retention is to choose a higher capacity cathode like an excess Li cathode material types [43]. Nevertheless, the use of high voltage cathode materials poses challenges of dissolution of transition metal ions which can “cross-over” to the anode and poison the SEI on anode. Improving the energy and power density of full cells with Si anode still requires further investigation particularly in the aspect of stabilizing the SEI, as we demonstrate that FEC helps improve cycling performance but it is not the optimum solution to the unstable Si anode SEI.

5. Conclusion

We have investigated the difference between standard carbonate electrolyte and FEC additive to the electrolyte on the electrochemical properties, electrode morphology, and surface chemistry of Si composite anode full cell. Electrochemical cycling performance and impedance of $LiPF_6$/EC/DEC degrade significantly after cycling. On the other hand, the presence of FEC tends to suppress this degradation reaction. $LiPF_6$/EC/DEC/FEC electrolyte leads to higher electrochemical performance and lower interfacial resistance on the Si composite anode full cell. It also exhibits superior reversibility at a higher scan rate. The SEI analyzed by XPS contains both organic and inorganic species. The Si anode cycled with FEC has an SEI that is inorganic components, with a large amount of LiF with less carbonate species. Both the electrochemical analysis (CV and EIS) and XPS gives further understanding that the kinetics of lithium ion migration can be controlled by the surface chemistry. All the above results indicate that these properties associated with the addition of FEC to the electrolyte influence the electrode surface morphology, forming less cracks. This leads to less overpotential during prolonged cycles and better cycle performance. This study provides the important insight of the interphase phenomenon for the Si composite anode full cell.

Acknowledgements

The majority of this work is funded by the Assistant Secretary for Energy Efficiency and Renewable Energy, Office of Vehicle Technologies, U.S. Department of Energy under Contract No. DE-AC02-05CH11231, Subcontract No. 7073923 under the Advanced Battery Materials Research (BMR) Program. H. S. and Y. S. M. are grateful for the partial funding from Asahi Kasei Corporation. J. A. and Y. Y. would like to thank Dr. Ich Tran for his help with the XPS experiments at the UC Irvine Materials Research Institute (IMRI) using instrumentation funded in part by the National Science Foundation Major Research Instrumentation Program under grant no. CHE-1338173. The SEM analysis in this work was performed at the San Diego Nanotechnology Infrastructure (SDNI), a member of the National Nanotechnology Coordinated Infrastructure, which is supported by the National Science Foundation (Grant ECCS-1542148).

Appendix A. Supplementary data

Supplementary data related to this article can be found at http://dx.doi.org/10.1016/j.jpowsour.2017.05.044.

References

[1] M. Armand, J.M. Tarascon, Nature 451 (2008) 652–657.
[2] J.M. Tarascon, M. Armand, Nature 414 (2001) 359–367.
[3] Y. Wang, J.Y. Lee, J. Phys. Chem. B 108 (2004) 17832–17837.
[4] Y. Liu, T. Matsumura, N. Imanishi, N. Ichikawa, A. Hirano, Y. Takeda, Electrochem. Commun. 6 (2004) 632–636.
[5] S.T. Chang, I.C. Leu, C.L. Liao, J.H. Yen, M.H. Hon, J. Mater. Chem. 14 (2004) 1821–1826.
[6] Y. Kim, Y. Yoon, D. Shin, J. Anal. Appl. Pyrolysis 85 (2009) 557–560.
[7] J. Li, J.R. Dahn, J. Electrochem. Soc. 154 (2007) A156–A161.
[8] L.Y. Beaulieu, K.W. Eberman, R.L. Turner, L.J. Krause, J.R. Dahn, Electrochem. Solid State Lett. 4 (2001) A137–A140.
[9] T.R. Hatchard, J.R. Dahn, J. Electrochem Soc. 151 (2004) A838–A842.
[10] B. PhiLiPpe, R. Dedryvère, J. Allouche, F. Lindgren, M. Gorgoi, H. Rensmo, D. Gonbeau, K. Edström, Chem. Mater. 24 (2012) 1107–1115.
[11] H. Wu, Y. Cui, Nano Today 7 (2012) 414–429.
[12] B. Liang, Y. Liu, Y. Xu, J. Power Sources 267 (2014) 469–490.
[13] P. Verma, P. Maire, P. Novák, Electrochim. Acta 55 (2010) 6332–6341.
[14] Z. Zhang, M. Zhang, Y. Wang, Q. Tan, X. Lv, Z. Zhong, H. Li, S. Fabing, Nanoscale 5 (2013) 5384–5389.
[15] S. Dalavi, P. Guduru, B.L. Lucht, J. Electrochem. Soc. 159 (2012) A642–A646.
[16] Y.M. Lin, K.C. Klavetter, P.R. Abel, N.C. Davy, J.L. Snider, A. Heller, C.B. Mullins, Chem. Commun. 48 (2012) 7268–7270.
[17] V. Etacheri, O. Haik, Y. Goffer, G.A. Roberts, I.C. Stefan, R. Fasching, D. Aurbach, Langmuir 28 (2012) 965–976.
[18] H. Nakai, T. Kubota, A. Kita, A. Kawashima, J. Electrochem. Soc. 158 (2011) A798–A801.
[19] K. Schroder, J. Alvarado, T.A. Yersak, J. Li, N. Dudney, L.J. Webb, Y.S. Meng, K.J. Stevenson, Chem. Mater. 27 (2015) 5531–5542.
[20] C.C. Nguyen, B.L. Lucht, J. Electrochem. Soc. 161 (2014) A1933–A1938.
[21] V. Baranchugov, E. Markevich, E. Pollak, G. Salitra, D. Aurbach, Electrochem. Commun. 9 (2007) 796–800.
[22] J. Ye, Y. Li, L. Zhang, X.P. Zhang, M. Han, P. He, H.S. Zhou, Appl. Mater. Interfaces 8 (2016) 208–214.
[23] L.F. Cui, Y. Yang, C.M. Hsu, Y. Cui, Nano Lett. 9 (2009) 3370–3374.
[24] N. Dupre, P. Moreau, E.D. Vito, L. Quazuguel, M. Boniface, A. Bordes, C. Rudisch, P.B. Guillemaud, D. Guyomard, Chem. Mater. 28 (2016) 2557–2572.
[25] K. Fridman, R. Sharabi, R. Elazari, G. Gershinsky, E. Markevich, G. Salitra, D. Aurbach, A. Garsuch, J. Lampert, Electrochem. Commun. 33 (2013) 31–34.
[26] S.D. Beattie, M.J. Loveridge, M.J. Lain, S. Ferrari, B.J. Polzin, R. Bhagat, R. Dashwood, J. Power Sources 302 (2016) 426–430.
[27] L. Liao, X. Cheng, Y. Ma, P. Zuo, W. Fang, G. Yin, Y. Gao, Electrochim. Acta 87 (2013) 466–472.
[28] E.M. Bauer, C. Bellito, M. Paquali, P.P. Prosoni, G. Righini, Electrochem. Solid State Lett. 7 (2004) A85–A87.
[29] F. Croce, A. D' Epifanio, J. Hassoun, A. Deptula, T. Olczac, B. Scrosati, Electrochem. Solid State Lett. 5 (2002) A47–A50.
[30] J. Shim, K.A. Striebel, J. Power Sources 119–121 (2003) 955–958.
[31] P. Liu, J. Wang, J.H. Garner, E. Sherman, S. Soukiazian, M. Verbrugge, H. Tataria, J. Musser, P. Finamore, J. Electrochem. Soc. 157 (2010) A499–A507.
[32] M. Koltypin, D. Aurbach, L. Nazar, B. Ellis, Electrochem. Solid State Lett. 10 (2007) A40–A44.
[33] M. Sina, J. Alvarado, H. Shobukawa, C. Alexander, V. Manichev, L. Feldman, T. Gustafsson, K.J. Stevenson, Y.S. Meng, Adv. Mater. Interfaces (2016) 1600438.
[34] H. Shobukawa, J.W. Shin, J. Alvarado, C.S. Rustomji, Y.S. Meng, J. Mater. Chem. 4 (2016) 15117–15125.
[35] N.S. Choi, K.H. Yew, K.Y. Lee, M. Sung, H. Kim, S.S. Kim, J. Power Sources 161 (2006) 1254–1259.
[36] M.H. Ryou, G.B. Han, Y.M. Lee, J.N. Lee, D.J. Lee, Y.O. Yoon, J.K. Park, Electrochim. Acta 55 (2010) 2073–2077.
[37] X. Chem, K. Gerasopoulos, J. Guo, A. Brown, C. Wang, R. Ghodssi, J.N. Culver, ACS Nano 4 (2010) 5366–5372.
[38] C. Xu, F. Lindgren, B. PhiLiPpe, M. Gorgoi, F. Björefors, K. Edström, T. Gustafsson, Chem. Mater. 27 (2015) 2591–2599.
[39] F.A. Soto, Y. Ma, J.M. Martinez de la Hoz, J.M. Seminario, P.B. Balbuena, Chem. Mater. 27 (2015) 7990–8000.
[40] H. Park, S. Choi, S. Lee, G. Hwang, N.-S. Choi, S. Park, J. Mater. Chem. A 3 (2015) 1325–1332.
[41] J.M. Martinez de la Hoz, P.B. Balbuena, Phys. Chem. Chem. Phys. 16 (2014) 17091–17098.
[42] K. Leung, S.B. Rempe, M.E. Foster, Y. Ma, J.M. Martinez de la Hoz, N. Sai, P.B. Balbuena, J. Electrochem. Soc. 161 (2014) A213–A221.
[43] H.D. Liu, D. Qian, M.G. Verde, M. Zhang, L. Baggeto, K. An, Y. Chen, K.J. Carrol, D. Lau, M. Chi, G.M. Veith, Y.S. Meng, Appl. Mater. Interfaces 7 (2015) 19189–19200.